JOURNAL OF GEOPHYSICAL RESEARCH, VOL. 112, D23S15, doi:10.1029/2006JD008113, 2007



# Aerosol modeling over Europe: 1. Interannual variability of aerosol distribution

E. Marmer[1,2] and B. Langmann[1,3]

Received 6 October 2006; revised 27 March 2007; accepted 24 April 2007; published 3 October 2007.

[1] Aerosol distribution over Europe has been simulated with a regional atmosphere-chemistry model. Primary and secondary organic and inorganic aerosols have been considered. The simulation was conducted for two different meteorological years 2002 and 2003 to analyze the spatial and temporal variability of the aerosol distribution. This paper focuses on the aerosol distribution, while the corresponding radiative forcing is described in the accompanying paper. Meteorological conditions play a major role in spatial and temporal variability in the European aerosol burden distribution. Regionally, year to year variability of monthly mean aerosol burden can reach up to 100% because of different weather conditions. The model evaluation against the source apportionment analysis shows that aerosols from fossil fuel combustion are well simulated. The evaluation suggests the importance of biomass burning emissions, which are not considered in the model simulations presented here. Because of lack of these emission sources and because of additional unknown formation processes of secondary organic aerosol, the carbonaceous aerosols are underestimated by a factor of 2–5 for black carbon and 10 for the organic carbon, respectively. Modeled sulfate aerosol is well represented.

**Citation:** Marmer, E., and B. Langmann (2007), Aerosol modeling over Europe: 1. Interannual variability of aerosol distribution, *J. Geophys. Res.*, *112*, D23S15, doi:10.1029/2006JD008113.

## 1. Introduction

[2] Atmospheric aerosol has significant effects on human health [e.g., *World Health Organization*, 2002], environment [e.g., *Stoddard et al.*, 1999] and climate [e.g., *Haywood and Boucher*, 2000]. In high-emission areas, such as Europe, an accurate description of regional aerosol burdens and their chemical nature is essential for the effectiveness of emission reduction policies [*Solmon et al.*, 2006] and air quality monitoring.

[3] This requires a detailed knowledge of the strength and regional distribution of the emission sources of primary aerosol particles and of the precursor gases involved in formation of secondary aerosol particles. Fossil fuel combustion is thought to be the major contributor to anthropogenic emissions in Europe for sulfur dioxide ($SO_2$), precursor of sulfate aerosol, black and primary organic carbon. The source apportionment analysis of continuous aerosol samples at five European sites indicates that biomass burning contributes an important part to primary carbonaceous aerosol concentration [*Gelencsér et al.*, 2007].

[4] Continuous efforts have been undertaken in the past to perform regional aerosol distribution simulations. Several Regional European Air Quality Models have been upgraded toward a more detailed description of tropospheric aerosols, evaluated by *Hass et al.* [2003]. All evaluated models include sulfate aerosol, while only two include carbonaceous aerosols, EURAD [*Hass et al.*, 1993, 1995] and LOTOS [*van Loon et al.*, 2000], being the only models explicitly treating secondary aerosol production utilizing the SORGAM module [*Schell*, 2000]. Simulations of primary and secondary carbonaceous aerosol and extensive evaluation against measurements have been performed utilizing the EMEP MSC-W Unified model [*Simpson et al.*, 2007]. Compared to global climate models the relatively high-resolution and detailed physical parameterizations offered by regional models are particularly suitable to describe the complexity of aerosol processes [*Solmon et al.*, 2006].

[5] Geographically localized sources and sinks and relatively short atmospheric lifetimes cause extreme spatial and temporal inhomogeneity of aerosol distribution and chemical composition [*Haywood and Boucher*, 2000]. Continuous aerosol measurements all over Europe (1991–2001) revealed significant interannual concentration variabilities of up to 30% [*Putaud et al.*, 2004]. *Hongisto et al.* [2003] applied a regional transport-chemistry model over Europe (1993–1998) and showed that the regional interannual variability of sulfur deposition strongly depends on the prevailing meteorological conditions. Hence, accurate modeling of meteorological conditions is necessary for the accurate prediction of the spatial and temporal variability of aerosol distribution.

[1] Max Planck Institute for Meteorology, Hamburg, Germany.
[2] Now at Institute for Environment and Sustainability, European Commission–Joint Research Centre, Ispra, Italy.
[3] Now at Department of Experimental Physics, National University of Ireland, Galway, Ireland.


0148-0227/07/2006JD008113$09.00

[6] We have utilized a regional atmosphere-chemistry model over Europe to simulate aerosol mass distribution for the years 2002 and 2003. Sulfate, black carbon and primary and secondary organic carbon aerosols have been included. The very different meteorological conditions for these years enable us to investigate their impact on aerosol column burden, including the impact on secondary particle formation. Evaluation of the modeled results with available measurements and source apportionment analysis of aerosol samples allows us to estimate the accuracy of predicted aerosol concentration distribution and to investigate the reasons for model deficiencies.

## 2. Experimental Setup

### 2.1. Atmosphere-Chemistry Model

[7] The regional atmosphere-chemistry model REMOTE (Regional Model with Tracer Extension [*Langmann*, 2000]) determines the physical and chemical state of the model atmosphere at every time step. A terrain following, hybrid pressure-sigma coordinate is used in the vertical with 19 vertical layers of unequal thickness between the ground and the 10 hPa pressure level. The horizontal resolution for the presented investigations is 0.5° on a spherical rotated grid. The dynamical part of the model is based on the global ECHAM 4 model [*Roeckner*, 1996; *Jacob*, 2001]. The prognostic equations for surface pressure, temperature, specific humidity, cloud water, horizontal wind components and trace species mass mixing ratios are written on an Arakawa-C-Grid [*Mesinger and Arakawa*, 1976]. In the current model setup, 63 chemical species are included. Considered aerosols, sulfate, black carbon and primary and secondary organic carbon, are treated as bulk mass. The species transport is determined by horizontal and vertical advection according to the algorithm of *Smolarkiewitz* [1983], convective updraft and downdraft by a modified scheme of *Tiedtke* [1989] and vertical diffusion after *Mellor and Yamada* [1974]. Dry deposition velocities are computed as by *Wesley* [1989] dependent on the friction velocities and stability of the lowest model layer. Wet deposition is computed according to *Walcek et al.* [1986] by integrating the product of the grid-averaged precipitation rate and the mean cloud water concentration. The gas phase chemistry package RADM II [*Stockwell et al.*, 1990] is implemented with a quasi-steady-state approximation (QSSA) solver [*Hesstvedt et al.*, 1978]. 43 longer-living prognostic species and 20 short living diagnostic molecules react in the gas phase. The photochemical gas phase mechanism consists of 158 reactions. Clear sky photolysis rates are calculated by a climatological preprocessor model [*Madronich*, 1987]. The presence of clouds modifies photolysis rates as described by *Chang et al.* [1987].

[8] At the first time step, REMOTE was initialized using meteorological analysis data of the European Center for Medium Range Weather Forecast (ECMWF), which were updated at the lateral boundaries every 6h. Chemical initial and boundary concentrations were prescribed by the model results of the global chemistry transport model MOZART *Horowitz et al.* [2003] for 14 species including PAN, $HNO_3$, $H_2O_2$, CO, NO, $NO_2$, $O_3$ and 7 hydrocarbons. Concentrations of the other species are derived from available measurements [*Chang et al.*, 1987, and references therein] and are held constant at the lateral model boundaries throughout the simulation.

### 2.2. Emissions

[9] Temporally variable emissions of $SO_x$, $NO_x$, $NH_3$, CO, VOC for the year 2001 and $PM_{2.5}$ emissions for the year 2000 were included in the 2002–2003 simulation. The emissions were provided by the Norwegian Meteorological Institute [*Vestreng*, 2003; *Vestreng et al.*, 2004], with monthly emission factors for each country and emission sector. Chemical speciation of $PM_{2.5}$ emissions into primary organic carbon (POC) and black carbon (BC) is based on *Andersson-Skøld and Simpson* [2001]. Recently, a new emission inventory for POC and BC became available from IIASA [*Bond et al.*, 2004]. Test simulations with prescribed IIASA emissions did not result in significantly different atmospheric concentration of carbonaceous aerosols.

[10] Anthropogenic VOC emissions are distributed in 12 different classes of volatile organic compounds (VOC) according to *Memmesheimer et al.* [1991]. Biogenic VOC emissions are calculated in REMOTE as a function of temperature, solar radiation and land use, based on the approach of *Guenther et al.* [1991, 1993]. We assume that 96% of the total $SO_x$ is emitted as $SO_2$ and 4% as $SO_4^{2-}$. $SO_x$ is emitted from natural and anthropogenic sources with DMS treated as $SO_x$. Natural sources of $NO_x$ are not considered. $SO_x$ and $NO_x$ emissions from point sources are distributed vertically between the seven lowest model levels following *Memmesheimer et al.* [1991].

### 2.3. Secondary Organic Aerosol Production

[11] In REMOTE, we consider secondary organic aerosol (SOA) production according to the approach of *Schell* [2000]. In this Secondary Organic Aerosol Model (SORGAM), gas/particle partitioning of interacting low vapor pressure products is treated as an absorption process into the organic mass of aerosol particles. The precursor gases, or volatile organic compounds (VOC), are of anthropogenic and biogenic origin (section 2.2). OH, $NO_3$ and $O_3$ oxidize these volatile gases to form semivolatile compounds. Little is known about detailed chemical reaction pathways of organic compounds leading to low-volatile products, which then partition between the gas phase and the particle phase to form SOA. In SORGAM, these processes are parameterized through measured and estimated stoichiometric coefficients that relate the reactive organic gases with semivolatile organic products. We consider products of aromatics, higher alkanes and higher alkenes. Isoprene is also thought to contribute to SOA formation under certain atmospheric conditions [*Limbeck et al.*, 2003; *Claeys et al.*, 2004]. We have not included products of isoprene, however, because very low aerosol yield of the isoprene products requires very high isoprene concentrations in order to generate substantial amount of secondary aerosol.

## 3. Model Results: Spatial and Temporal Variations of the Aerosol Load

### 3.1. Impact of Emissions on the Variation of the Aerosol Load

[12] Figure 1 shows monthly mean emissions and respective atmospheric loads for black and primary organic

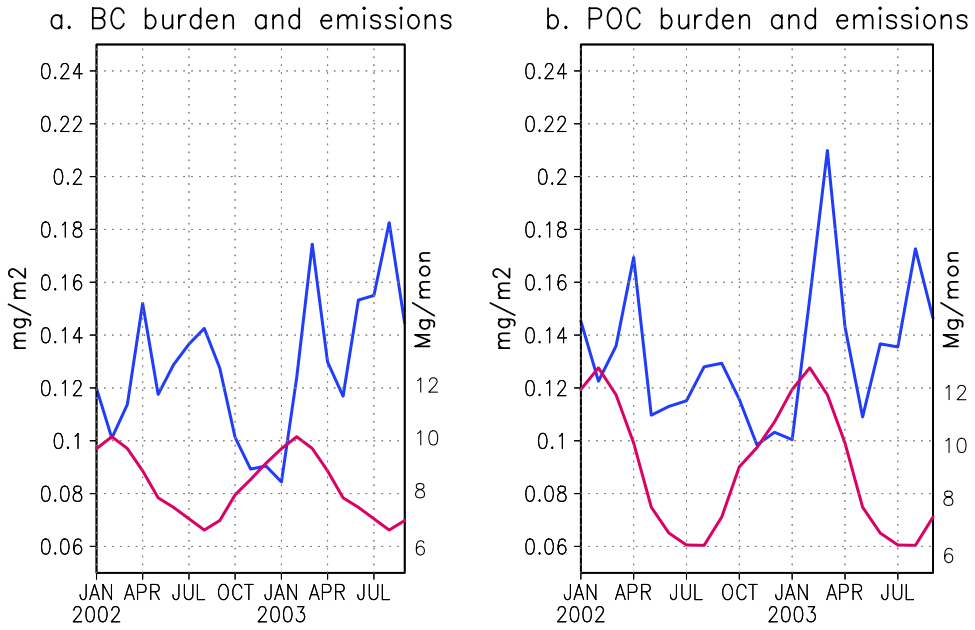


**Figure 1.** Time series of monthly mean emission fluxes (Mg(mon$^{-1}$) per grid cell) (red) and primary aerosol column load (mg(m$^{-2}$)) (blue), both averaged over the model domain: (a) BC and (b) POC.

carbon. The same emission inventory was applied 2002 and 2003, with an emission maximum in February and minimum in August for both carbonaceous species. In 2002, the burden maximum of both occurred in April, the minimum in November. The burden of BC in February (emission maximum) was much lower than in August (emissions minimum). The burden of POC for February and August were nearly the same for each year, but very different between years, despite consistently low emission levels in August. In 2003 the burden maximum for BC occurred in August, coinciding with emissions minimum; the burden maximum for POC occurred in March, with a secondary maximum in August. On the European average, the temporal variation of the atmospheric burden of primary carbonaceous aerosols show large interannual variability and do not primarily depend on the temporal variation of the emission sources.

[13] Figure 2 shows the variability of the emissions of precursor gases $SO_x$ and anthropogenic VOCs, and the column burden of secondary aerosols, sulfate aerosol and anthropogenic SOA, respectively. The temporal variation of

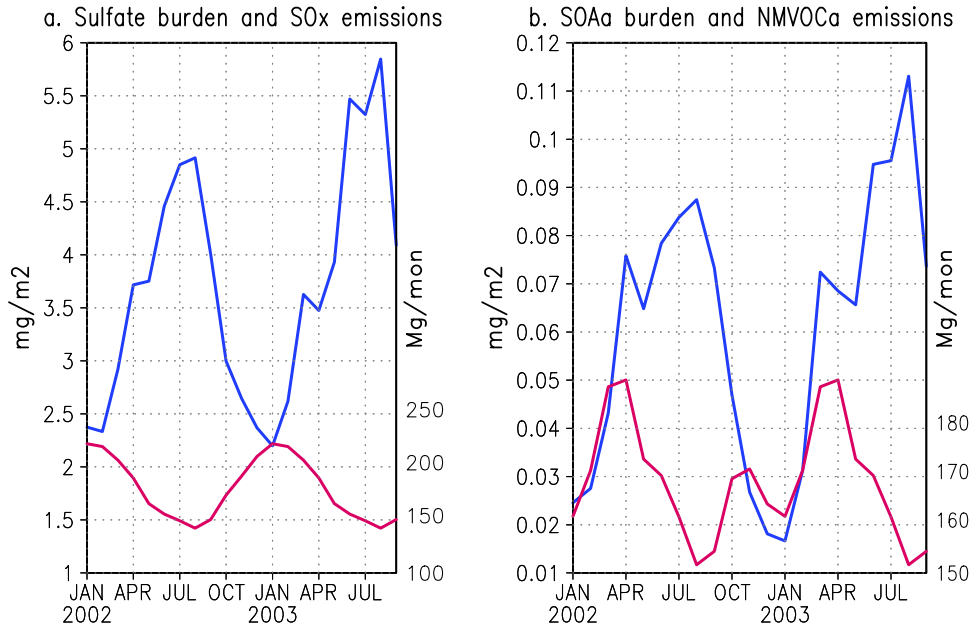


**Figure 2.** Time series of monthly mean emission fluxes of precursor gases (Mg(mon$^{-1}$)) (red) and secondary aerosol column load (mg(m$^{-2}$)) (blue), both averaged over the model domain: (a) $SO_x$ and sulfate and (b) anthropogenic NMVOC and anthropogenic SOA.

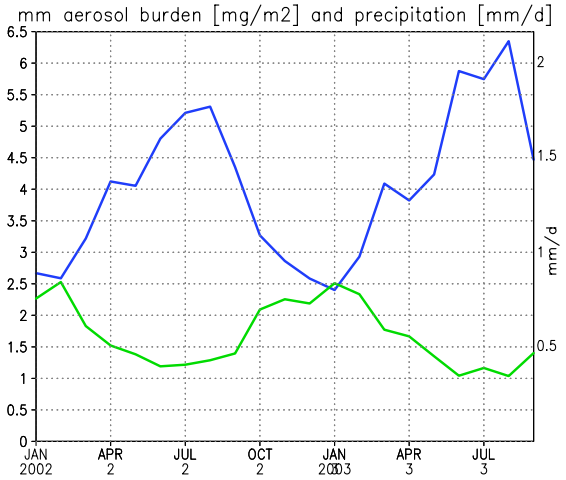


**Figure 3.** Time series of monthly mean precipitation ($mm(d^{-1})$) (green) and total aerosol burden (containing sulfate, black carbon, primary and secondary organic carbon) ($mg(m^{-2})$) (blue), both averaged over the model domain.

sulfate shows an anticorrelation with $SO_x$ emissions: here the emissions maxima in January coincide with burden minima, and the emissions minima in August with burden maxima for both years. The VOC emissions have a very different annual cycle compared to that of $SO_x$, with a maximum in March/April, a secondary maximum in October/November, a minimum in August and a secondary minimum in January. The secondary organic aerosol burden trend follows that of emissions from November to March; the trend is opposite otherwise. Despite the very different emission patterns, the annual cycle of SOA resembles that of sulfate. Both species are subjected to interannual variability, with higher aerosol loads in summer 2003 compared to 2002.

[14] There is an enhanced aerosol burden for all species in April 2002 and in March 2003, that is not reflected in the emissions.

### 3.2. Impact of Meteorological Conditions on Variations of the Aerosol Load

[15] The temporal and spatial variation in aerosol load is governed to great extent by meteorological conditions, which determine advection, turbulent diffusion, convective transport and dry and wet deposition. Wet deposition is the main removal process of aerosol from the atmosphere. The scavenging efficiency in the model depends on hygroscopicity of the particles and liquid water content in the atmosphere based on *Kasper-Giebl et al.* [2000] and *Hitzenberger et al.* [2000]. The scavenging efficiency for black carbon is assumed to be 3 times smaller than for hygroscopic particles (i.e., sulfate and organic carbon; A. Kasper-Giebl, personal communication, 2007). Sensitivity studies have shown, that assuming BC to be hygroscopic, i.e., having same scavenging efficiency as sulfate, results in up to 10% decrease in the simulated atmospheric BC concentration. This sensitivity however, has no impact on our conclusions regarding the dependency of the atmospheric aerosol load on meteorological conditions and on emissions. Spatially averaged monthly mean total aerosol load (containing sulfate, black carbon, primary and secondary organic carbon) was found to strongly anticorrelate with monthly precipitation (Figure 3). Seasonal and interannual variability of the mean precipitation in Europe is directly reflected in the European mean pollution level with pollution maximum (precipitation minimum) in August 2003 and pollution minimum (precipitation maximum) in January 2003.

[16] To illustrate the dependency of interannual variation of the aerosol burden on pressure, wind and regional precipitation patterns, we have analyzed February and August 2002 and 2003. These two months demonstrate high interannual variability in aerosol burden (Table 1).

#### 3.2.1. February

[17] The general weather conditions of February 2002 were characterized by a low-pressure system north of Scandinavia with steep pressure gradients over north-central Europe, transporting North Atlantic air masses with westerly winds toward the European continent (Figure 4). Strong advection occurred in areas with strong emissions (not shown). A high-pressure system with weak pressure gradients was located over southern Europe. In contrast, in February 2003, there was a blocking-high over western Russia, with calm winds, inducing very little advection. This high-pressure system was complemented by an Iceland low. Relatively unpolluted air from the North Atlantic could not reach the European continent, just striving the northern coasts. The main emission sources are located in the region of the blocking high. The difference plots of the sea level pressure and aerosol load between February 2002 and February 2003 reveal an anticorrelation, in areas with significant emission sources. The regions of negative (positive) pressure differences show positive (negative) difference in aerosol load. There is also an anticorrelation between the aerosol load and precipitation differences in these two Februaries. In February 2002, there was strong precipitation over northern Scandinavia, Russia, north UK and the Alpine Region (over 220 $mm(month^{-1})$), moderate precipitation over northern Europe, and little or no precipitation in the south. In February 2003, there was less precipitation over all of Europe, except in the south, where there was more precipitation over the Black Sea, the Balkans, Turkey and the eastern Mediterranean.

[18] As a result of these weather conditions: strong advection, atmospheric instability and strong precipitation in February 2002 versus atmospheric stability of the blocking-high, low advection and low precipitation in February 2003, the aerosol load over central Europe, close to strongest emission sources, is 2 to 6 $mg(m^{-2})$ higher in February 2003 than in the previous year. Only over areas with stronger precipitation and higher sea level pressure in

**Table 1.** Mean Aerosol Burden in February and August 2002 and 2003[a]

| Aerosol Type | Feb 2002 | Feb 2003 | Aug 2002 | Aug 2003 |
|---|---|---|---|---|
| Sulfate | 2.30 | 2.60 | 4.90 | 5.80 |
| SOA | 0.03 | 0.04 | 0.13 | 0.15 |
| POC | 0.12 | 0.15 | 0.14 | 0.17 |
| BC | 0.10 | 0.12 | 0.13 | 0.18 |

[a]Unit is $mg(m^{-2})$.

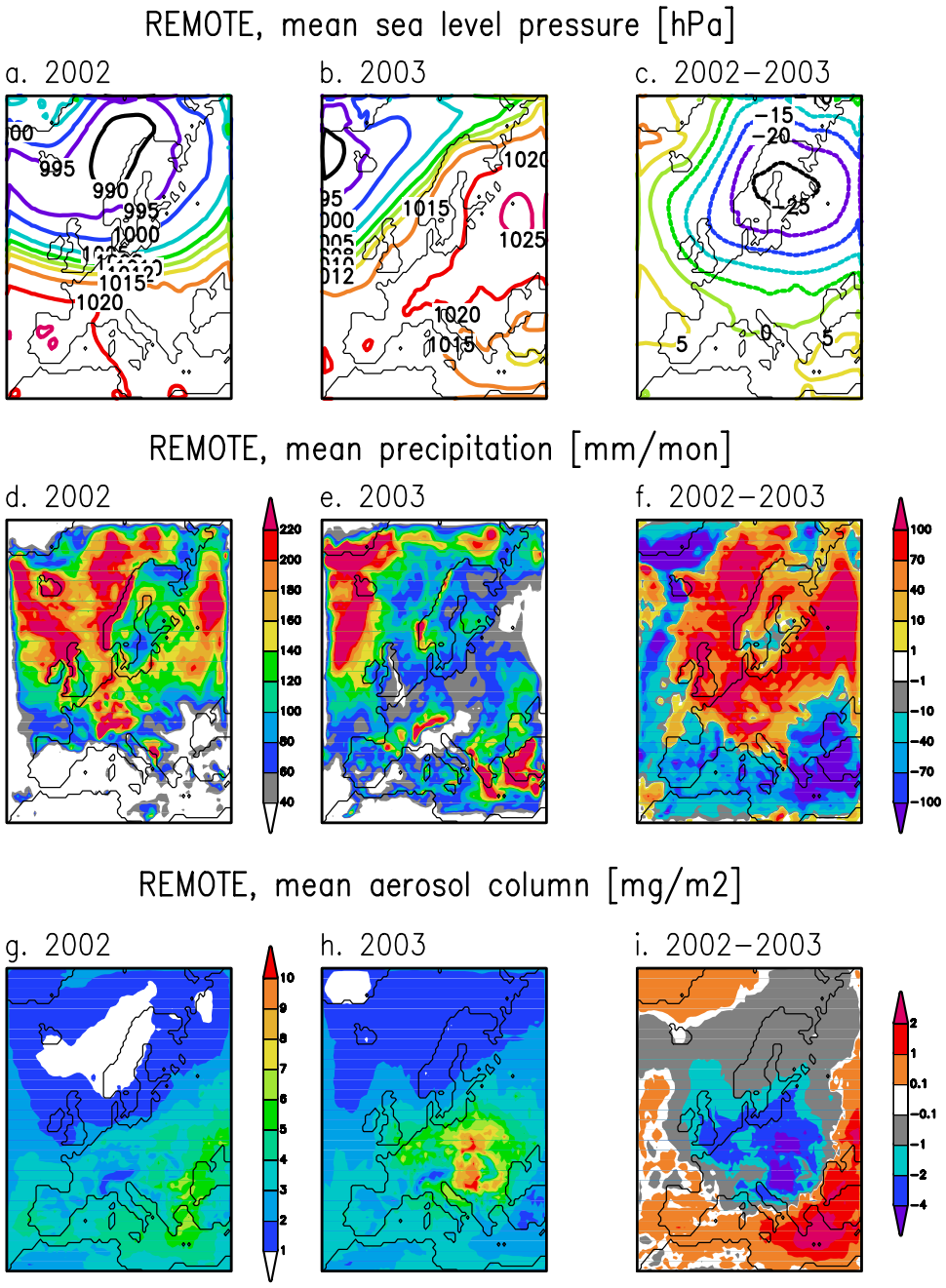


**Figure 4.** Monthly mean meteorology versus monthly mean aerosol column load for February 2002 and 2003: Monthly mean sea level pressure for February (a) 2002 and (b) 2003 and (c) pressure difference 2002–2003 (hPa); monthly precipitation for February (d) 2002 and (e) 2003 and (f) precipitation difference 2002–2003 (mm(mon$^{-1}$)); and monthly mean total aerosol column load for February (g) 2002 and (h) 2003 and (i) aerosol column load difference 2002–2003 (mg(m$^{-2}$)).

February 2003, as was found in the south, were the aerosol loads lower than in 2002 (1–2 mg(m$^{-2}$) less).

### 3.2.2. August

[19] The anticorrelation between the difference in sea level pressure and aerosol load observed for the two Februaries also holds true for August 2002 and 2003 (Figure 5). The magnitude of the difference in aerosol load is the same as in February, but the distribution is opposite: only Scandinavia and northern Russia were more polluted in August 2002 than in 2003. Central Europe was more polluted in August 2003, and the Mediterranean region shows 4–6 mg(m$^{-2}$) more aerosol burden than in the previous year. The winds were very calm for both years. The summer of 2003 was marked by semiarid conditions almost all over Europe. August was the driest month with mean precipitation of less then 5 mm(month$^{-1}$). It is important to mention that the arid conditions led to extended forest fires in Portugal, Spain and France, significantly enhancing pollution, but the biomass emissions are not included in our emission inventory. Hence, we expect the

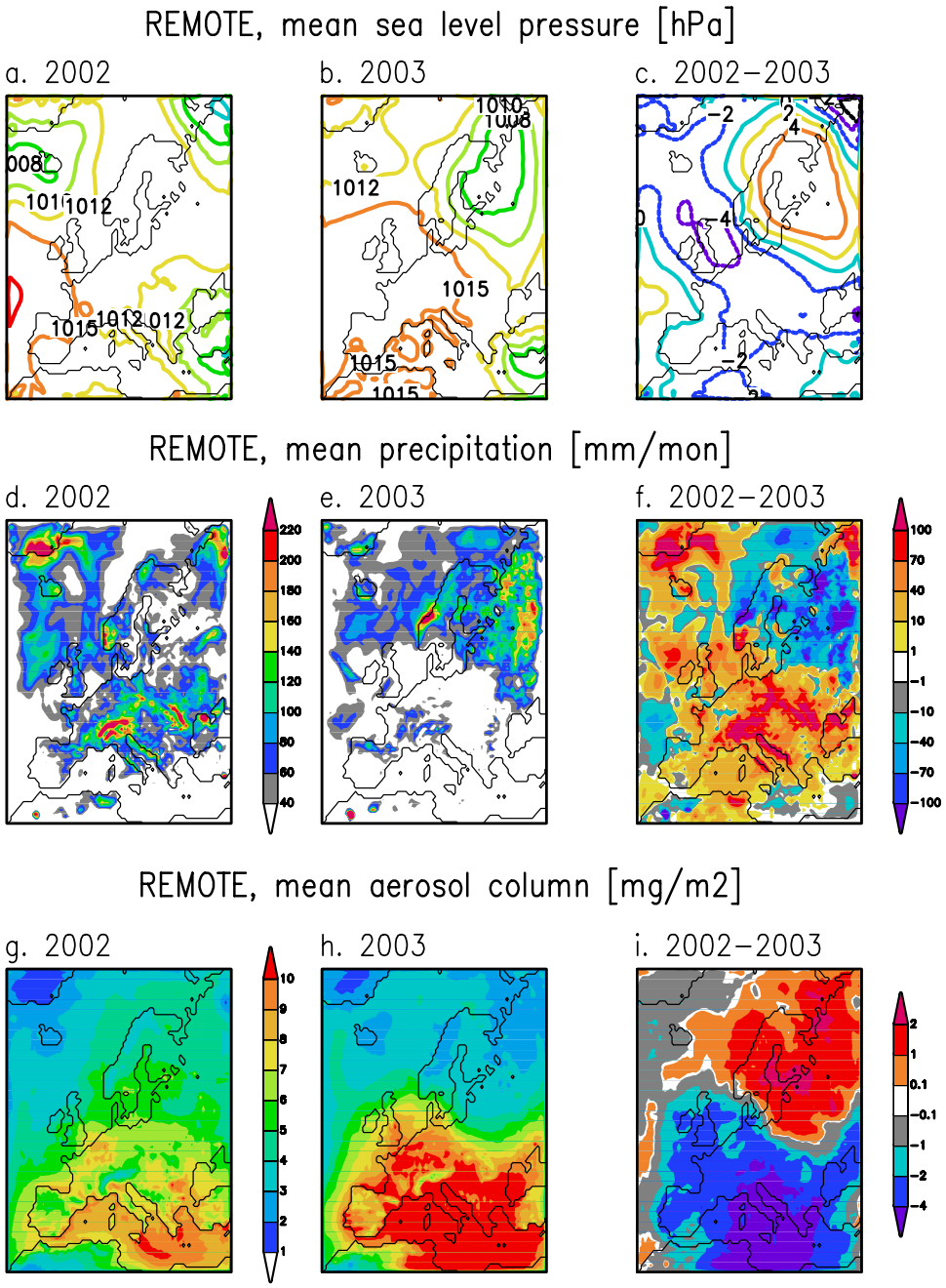


**Figure 5.** Monthly mean meteorology versus monthly mean aerosol column load for August 2002 and 2003: Monthly mean sea level pressure for August (a) 2002 and (b) 2003 and (c) pressure difference 2002–2003 (hPa); monthly precipitation for August (d) 2002 and (e) 2003 and (f) precipitation difference 2002–2003 (mm(mon$^{-1}$)); and monthly mean total aerosol column load for August (g) 2002 and (h) 2003 and (i) aerosol column load difference 2002–2003 (mg(m$^{-2}$)).

summer pollution in southern Europe to be even higher then simulated. Only in Scandinavia, Russia and Ukraine did some precipitation fall. The precipitation pattern is almost exactly opposite to that of August 2002. The model does not capture the floods in August 2002, the simulated precipitation amount is not unusual for this time of the year. The modeled precipitation pattern is strongly reflected in the aerosol load distribution. While the aerosol load is higher over Scandinavia and east-northern Russia in August 2002, the opposite is true for the rest of Europe in August 2003.

### 3.3. Impact of Meteorological Conditions on the Formation of Secondary Aerosols

[20] We showed in section 3.2 that atmospheric stability and precipitation play a key role for the spatial and temporal aerosol atmospheric burden variation. For secondary aerosol particles, the influence of meteorological conditions goes much further: the formation of these aerosols in the atmosphere depends on several meteorological parameters, including liquid water content, incoming solar radiation and air temperature. $SO_2$ is converted to sulfate via both

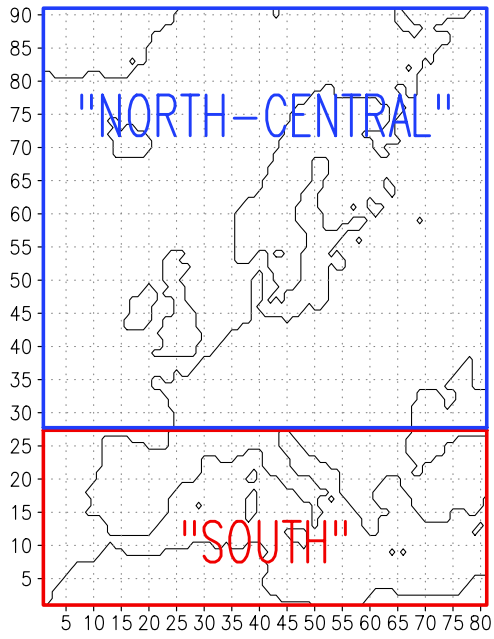


**Figure 6.** Map of the selected areas "north-central" and "south."

aqueous and gaseous phase chemical reactions. For conversion in cloud water, clouds and liquid water must be present. The regional patterns of total cloud cover and the vertically integrated liquid water content are very similar to that of precipitation; thus areas of aerosol formation in clouds overlap with those of aerosol removal by precipitation. To be able to distinguish the influence of each process, we have looked at different atmospheric levels. From the temporal variability of the sulfate aerosol distribution (not shown), we can clearly distinguish between two regions: northern and central Europe (further called "north-central") and southern Europe (further called "south") (Figure 6). For "north-central," sulfate concentration follows the trend in liquid water content in the lower atmosphere below the clouds (Figure 7a), showing the dependency of sulfate production on the availability of liquid water. At cloud level, as an example at approximately 800 hPa (Figure 7b), the trend of sulfate concentration is quite opposite to that of liquid water content, indicating that removal processes dominate over production. For "south," the opposite trend at the cloud level can also be found. The dependency of sulfate concentration on the liquid water content in the lower atmosphere however, is less significant, than in "north-central." We conclude that the aqueous production of sulfate is the dominant formation mechanism in northern and central Europe in the lower atmosphere. At the cloud level, aerosol removal dominates over aerosol production. In southern Europe, aqueous production is by far less important.

[21] For sulfate and secondary aerosol production, photooxidation plays a major role. Availability of $O_3$, OH and $NO_3$ in the atmosphere depends on temperature and solar radiation. For "north-central," sulfate concentration is independent of surface solar radiation and air temperature (Figure 8). For "south," the surface sulfate concentration shows significant dependency on the surface solar radiation

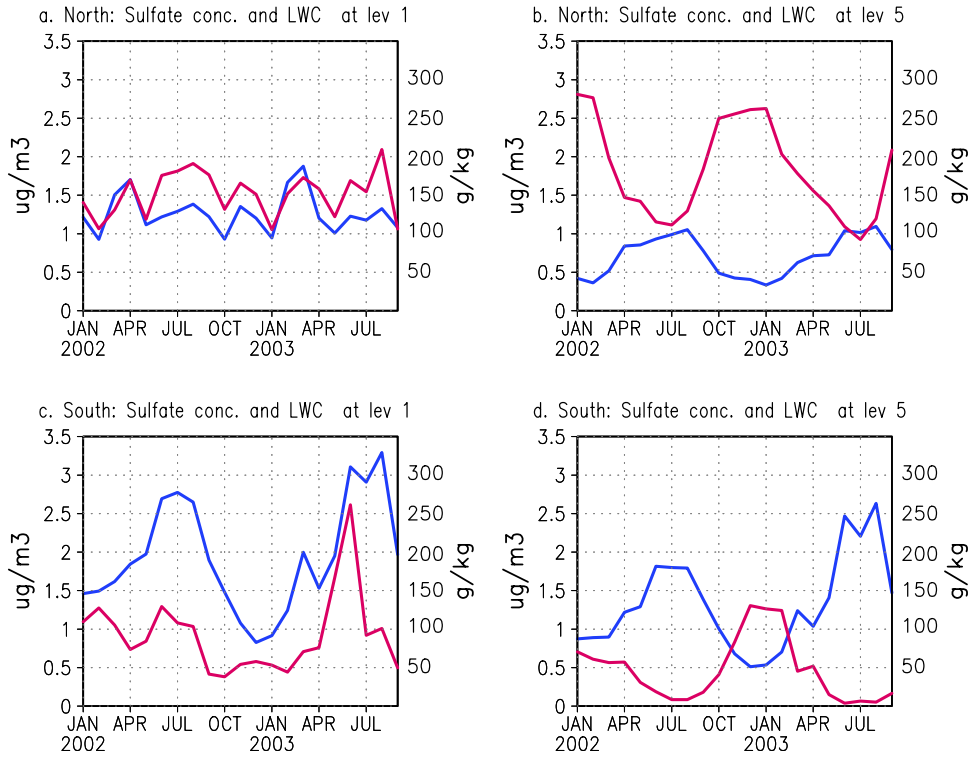


**Figure 7.** Time series of liquid water content ($g(kg^{-1})$) (red) and sulfate aerosol concentration ($\mu g(m^{-3})$) (blue): (a) "north-central" at the surface level, (b) "north-central" at approximately 800 hPa, (c) "south" at the surface level and (d) "south" at approximately 800 hPa.

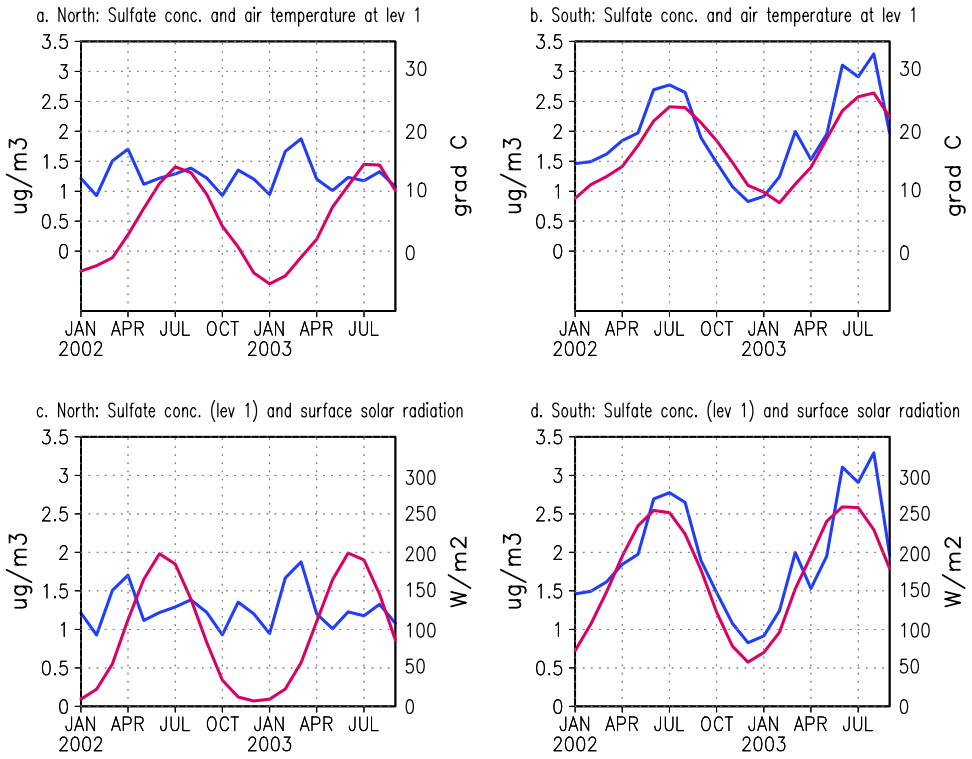


**Figure 8.** Time series of temperature (°C) (red) and sulfate aerosol concentration ($\mu g(m^{-3})$) (blue): (a) "north-central" and (b) "south." Timer series of surface solar radiation (W $m^{-2}$) (red) and sulfate aerosol concentration ($\mu g(m^{-3})$) (blue): (c) "north-central" and (d) "south."

and air temperature. We conclude that in southern Europe photo-oxidation is the dominant mechanism of sulfate production. Figure 9 shows the dependency of the surface SOA concentration on the air temperature surface solar radiation. Generally, enhanced temperatures lead to enhance SOA concentrations (except in April 2002 and March 2003).

## 4. Model Evaluation Against Observations

### 4.1. Sulfate Aerosol

[22] The model was evaluated against observations from Cooperative Programme for Monitoring and Evaluation of the Long-Range Transmissions of Air Pollutants in Europe (EMEP) [*Hjellbrekke*, 2004] (Figure 10). There is a large scatter for all seasons. The best agreement is found for spring and fall 2002. In summer, the lower end values (<0.6 $\mu g(S)m^{-3}$) are well represented by the model, while the higher values are underestimated. The largest scatter was found in winter. It must be kept in mind that it is difficult to compare point measurements with model of 0.5° resolution.

[23] Aerosol measurements obtained during the EU-Project CARBOSOL [*Gelencsér et al.*, 2007] at five sites: Sonnblick, Puy De Dome, Schauinsland, Aveiro and K-Puszta, were also compared with the model results (Figure 11). The detailed description of the sampling sites, sampling and analyzes are given by *Pio et al.* [2007]. We have chosen a higher model level for the three elevated sites, to compare modeled and observed aerosol concentrations at the free troposphere. We have simulated the years 2002 and 2003, while the observations were obtained for the years 2003 and 2004, so we compare the observed and modeled concentrations for the year 2003. In both, the modeled and observed concentrations, interannual variability can be observed at all sites.

[24] The annual variability of sulfate aerosol concentration is very well captured by REMOTE. At the southwestern (Aveiro) and the three central European sites maxima during the summer and minima during the winter are visible in the modeled and observed data sets. The annual variability is reversed at the southeastern European site K-Puszta, where the concentration increases during wintertime. High $SO_x$ emissions from domestic heating result in enhanced wintertime sulfate aerosol pollution. At K-Puszta, REMOTE can reproduce the concentration increase during winter but does not capture the very high value of 4.5 $\mu g(S)m^{-3}$ in February 2003.

### 4.2. Carbonaceous Aerosols

[25] Simulated concentrations of BC at the CARBOSOL sites were compared with measurements (Figure 12). Total organic carbon was compared with simulated total and primary organic carbon in Figure 13, where the modeled values were multiplied by a factor of 10. The model clearly underpredicts both carbonaceous species. Reasons for this underestimation can be sought in the source apportionment analysis of the CARBOSOL samples [*Gelencsér et al.*, 2007]. The sampled species were specified as emitted from fossil fuel combustion and from biomass burning. Keeping in mind that biomass burning emissions are not included in our emission inventory, we have compared the modeled BC and POC with sampled BC and POC appointed to fossil fuel

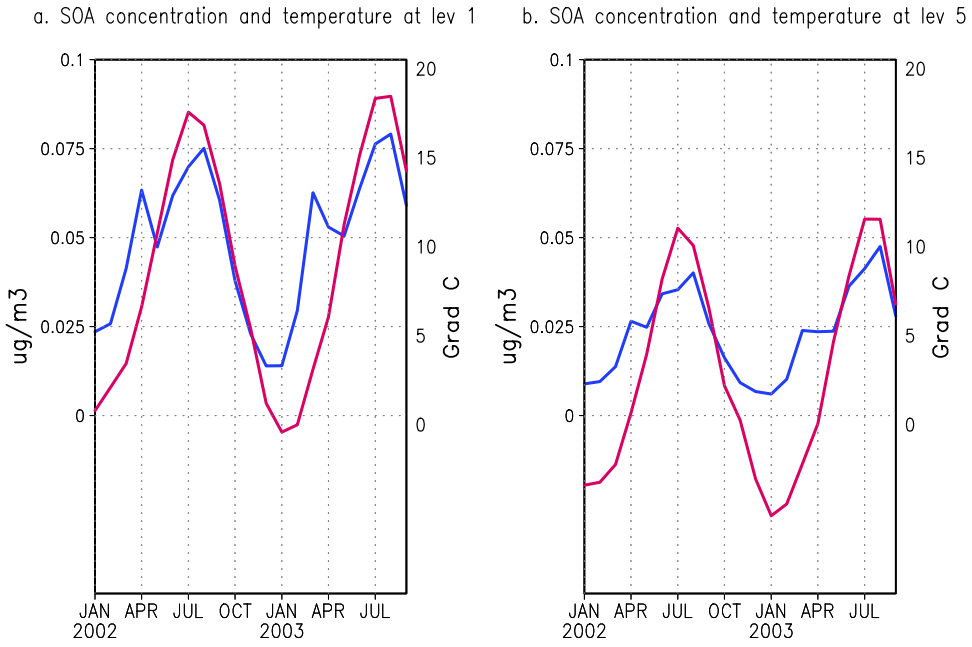


**Figure 9.** Time series of temperature (°C) (red) and SOA concentration ($\mu$g(m$^{-3}$)) (blue): (a) the surface level and (b) at approximately 800 hPa.

combustion and find a much better agreement (Table 2). Good agreement between modeled and sampled fossil fuel BC was found for Schauinsland and K-Puszta. At Sonnblick, the modeled concentration during winter is overestimated by a factor of 4, probably because of this high site's elevation. The site may represent the free troposphere during winter time inversion conditions, which could not be captured by the model. The BC concentration is under-

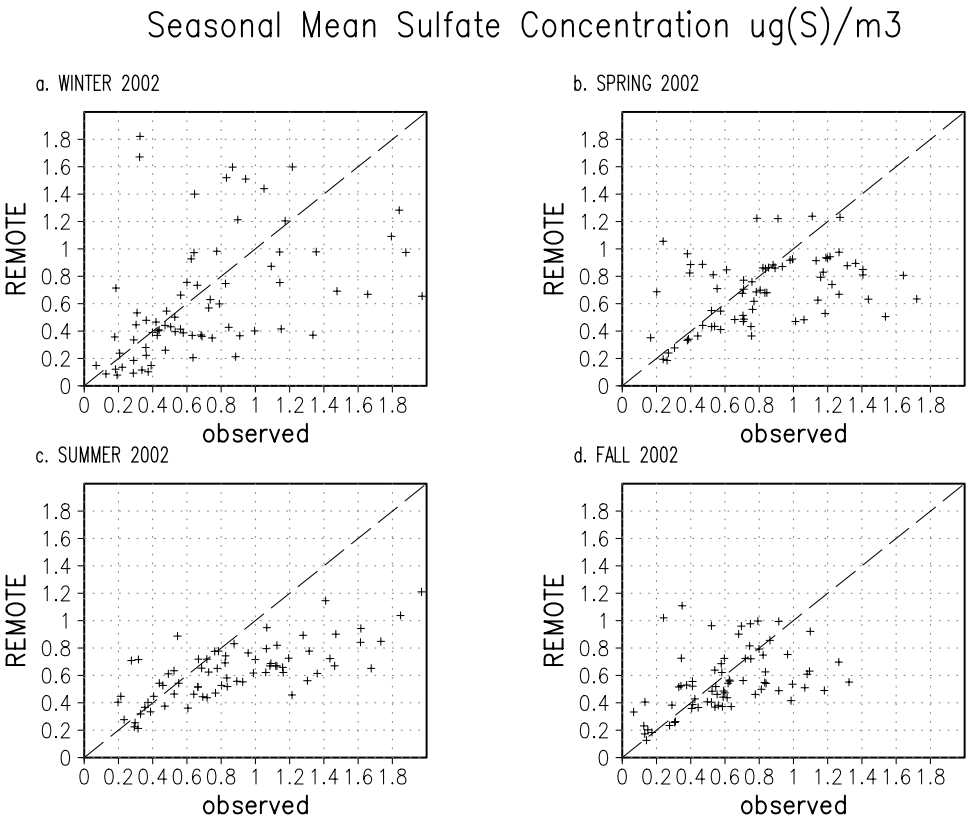


**Figure 10.** Observed versus modeled surface sulfate concentration ($\mu$g(S)m$^{-3}$) at 74 EMEP sites [*Hjellbrekke*, 2004]: (a) winter 2002, (b) spring 2002, (c) summer 2002, and (d) fall 2002.

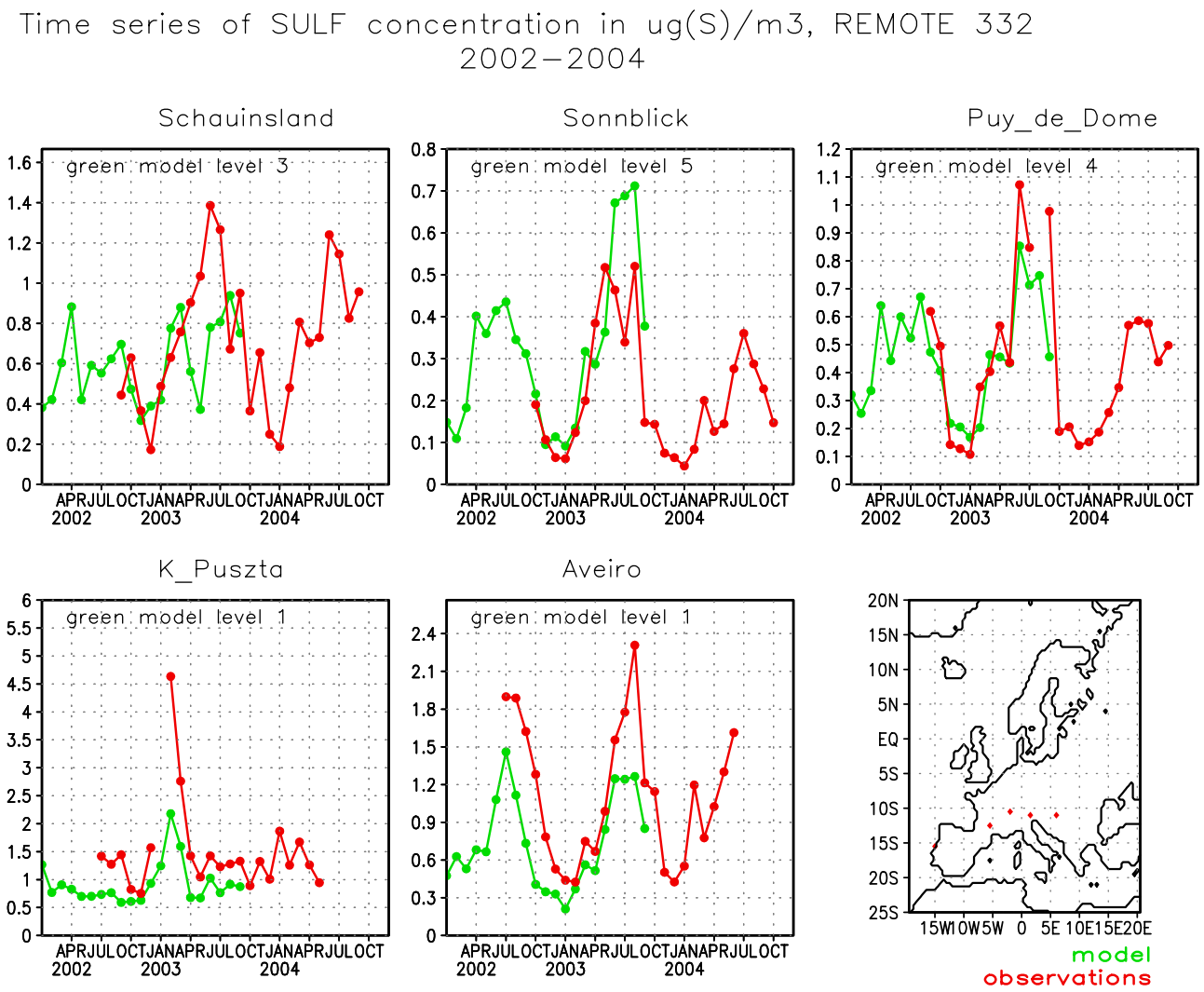


**Figure 11.** Observed (red) versus modeled (green) monthly mean time series of sulfate concentration ($\mu$g(S)m$^{-3}$) at five CARBOSOL sites. Map of the observational sites, from left to right: Aveiro, Puy de Dome, Schauinsland, Sonnblick, and K-Puszta.

estimated by a factor of 2 at Puy de Dome during both seasons and at Aveiro during summer. During winter, the contribution of BC originating from biomass burning is very prominent at Aveiro (85%) and at K-Puszta (41%); for other sites this contribution varies from 8 to 20% [*Gelencsér et al.*, 2007]. Our not considering biomass burning emissions in the emission inventory explains the underestimation of BC by REMOTE to a certain extend. For OC, the analysis goes even further, trying to identify primary and secondary organic aerosols. Similar to BC, modeled POC concentrations agree well with the POC amounts apportioned to the fossil fuel combustion at Schauinsland and K-Puszta. At Sonnblick, the POC concentration is again overestimated by a factor of 2 in winter. At Puy de Dome, it is underestimated by a factor of 4 in winter and a factor of 2 in summer, as well as at Aveiro by a factor of 2.5 in summer. The POC from biomass burning is found to contribute almost 90% of the primary organic aerosols in Aveiro and K-Puszta in winter, and approximately 50% for other sites for winter and summer. Simulated SOA concentration is extremely underpredicted by one to two (at Aveiro) orders of magnitude (not shown). In summer, very high contribution of SOA from nonfossil sources was found in most CARBOSOL samples. This includes not only SOA from VOC emitted by vegetation, but also from VOC emitted by biomass burning. Thus, biomass burning emissions contribute not only to primary, but also to secondary carbonaceous aerosol concentration. It is important to mention, that the concept of SOA given by *Gelencsér et al.* [2007] differs from ours and includes condensation of directly emitted semivolatile organic compounds at low ambient temperatures and also covers primary emissions from nonspecific sources. That is why observed contribution of SOA remains relatively high during wintertime, and cannot be directly compared with simulated SOA concentration.

[26] Annual mean concentration of each aerosol species were also compared with mean values obtained by *Putaud et al.* [2004]. In this work, chemical composition of aerosol samples collected from different European sites over the past decade have been analyzed. Table 3 shows the range of the absolute annual mean concentrations of sulfate, black and organic carbon aerosol in $PM_{2.5}$ from natural, rural and near-

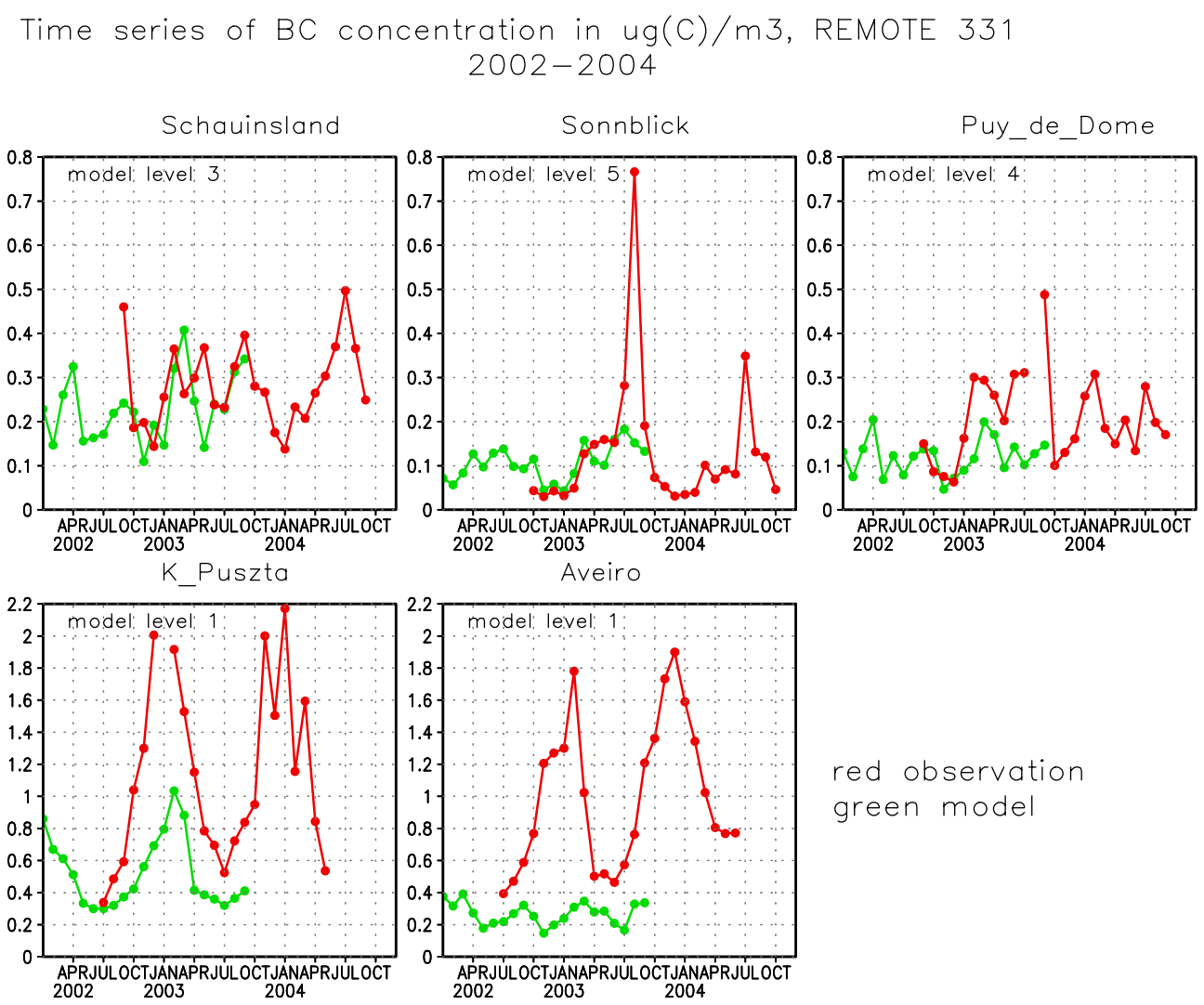


**Figure 12.** Observed (red) versus modeled (green) monthly mean time series of BC concentration ($\mu$g(S)m$^{-3}$) at five CARBOSOL sites: Schauinsland, Sonnblick, Puy de Dome, K-Puszta, and Aveiro.

city sites compared to the simulated annual mean concentration. The simulated annual mean for sulfate aerosol is within the range measured; black carbon is underpredicted by at least a factor of 3, and organic carbon by an order of magnitude.

## 5. Conclusions

[27] The regional atmosphere-chemistry model REMOTE [*Langmann*, 2000] has been applied for two very different meteorological years to determine spatial and temporal variability of the aerosol column load and the aerosol direct forcing. Model results compared with measurements showed that ground level sulfate aerosol concentrations and variability could be successfully simulated, but the simulation of the carbonaceous species remains a challenge. Carbonaceous compounds from fossil fuel are well predicted for some sites, while underpredicted by a factor of 2 to 3 for others. Carbonaceous emissions from biomass burning must be included in the model: their exclusion from our emissions partially explains the tremendous underprediction of total black and organic carbon concentrations. Gas-particle partitioning of oxidized semivolatile organic compounds alone cannot explain the dominant contribution of SOA to total organic mass. Surprisingly high contribution of SOA in winter observed in samples could not at all be captured by the model. Secondary organic carbon is further underpredicted by the model because of missing formation processes that are yet not fully understood. Generally, we estimate the underprediction factor of total black carbon ranging from 2 to 5, and the underprediction factor of the organic matter to be an order of magnitude. The underprediction of black carbon also agrees with the study of *Schaap et al.* [2004], suggesting that BC emissions for Europe are underestimated by a factor of 2.

[28] The temporal variability of emission sources of sulfate and primary carbonaceous aerosols are not directly reflected in the variability of the aerosol burden. Meteorological conditions play a major role in the spatial and temporal variations of the aerosol burden distribution. The main removal process of aerosol from the European atmosphere is wet deposition, thus the aerosol burden is very sensitive to precipitation. In general, pressure systems and

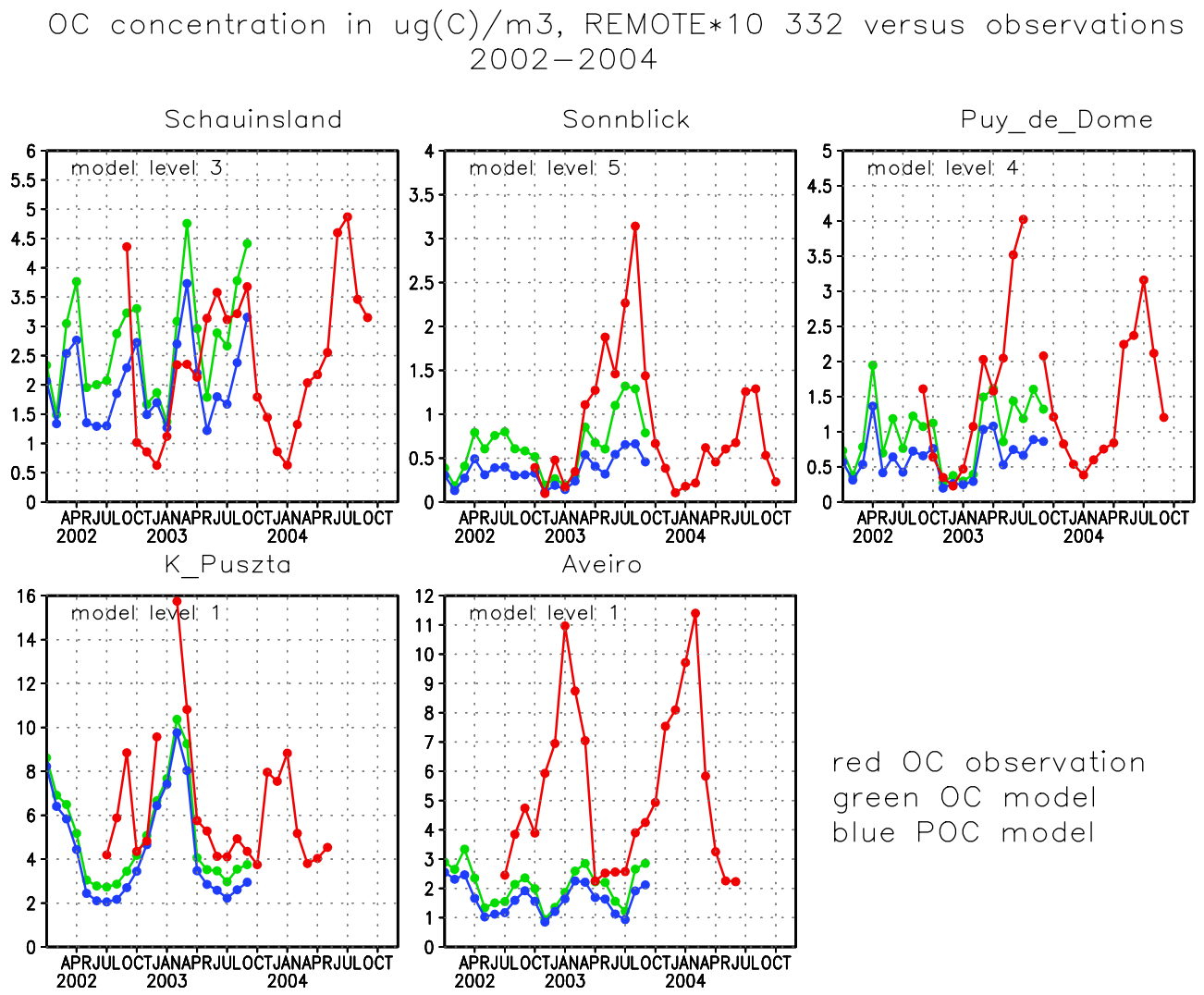


**Figure 13.** Observed monthly mean TOC concentration (red) versus modeled monthly mean TOC (green) and POC (blue) concentration multiplied by 10 ($\mu$g(S)m$^{-3}$) at five CARBOSOL sites: Schauinsland, Sonnblick, Puy de Dome, K-Puszta, and Aveiro.

**Table 2.** Seasonal Mean BC and POC From Fossil Fuel Combustion [*Gelencsér et al.*, 2007] Compared With Modeled BC and POC at CARBOSOL Sites[a]

| CARBOSOL Site | $BC_{ff}$, [b]Winter | BC Modeled, Winter 2002/2003 | $BC_{ff}$, [b]Summer | BC Modeled | |
|---|---|---|---|---|---|
| | | | | Summer 2002 | Summer 2003 |
| Aveiro | 0.307 | 0.249 | 0.518 | 0.232 | 0.235 |
| K-Puszta | 1.023 | 0.841 | 0.471 | 0.307 | 0.348 |
| Schauinsland | 0.241 | 0.219 | 0.237 | 0.185 | 0.259 |
| Puy de Dome | 0.197 | 0.092 | 0.276 | 0.108 | 0.124 |
| Sonnblick | 0.016 | 0.061 | 0.114 | 0.122 | 0.165 |
| CARBOSOL Site | $POC_{ff}$, [b]Winter | POC Modeled, Winter 2002/2003 | $POC_{ff}$, [b]Summer | POC Modeled | |
| | | | | Summer 2002 | Summer 2003 |
| Aveiro | 0.178 | 0.170 | 0.301 | 0.130 | 0.132 |
| K-Puszta | 0.593 | 0.787 | 0.273 | 0.210 | 0.245 |
| Schauinsland | 0.140 | 0.184 | 0.138 | 0.148 | 0.195 |
| Puy de Dome | 0.114 | 0.027 | 0.160 | 0.060 | 0.077 |
| Sonnblick | 0.009 | 0.019 | 0.066 | 0.036 | 0.062 |

[a]Values given in $\mu$g(C)m$^{-3}$.
[b]From fossil fuel combustion [*Gelencsér et al.*, 2007].

**Table 3.** Annual Mean Surface Concentration of Sulfate and Black and Organic Carbon Over Europe[a]

| Author | Sulfate | BC | OC |
|---|---|---|---|
| *Putaud et al.* [2004] in $PM_{2.5}$ | 1–3 | 0.5–2 | 0–6 |
| Model results, this study | 1.42 | 0.18 | 0.23 |

[a]Unit is $\mu g(m^{-3})$.

corresponding winds control the advection and vertical diffusion and/or accumulation of aerosols. Blocking highs over areas of strong emissions enhance pollution levels substantially. Westerly winds from the North Atlantic, associated with strong pressure gradients, reduce pollution despite strong emissions. A combination of both removal by precipitation and enhanced advection can reduce the monthly mean burden by a factor of two, as was demonstrated for the month of February 2002 versus 2003. Semiarid conditions in the summer of 2003 strongly affected the pollution levels, especially in lower latitudes. Despite the fact that extreme precipitation events in August 2002 could not be captured well by the model, and that the pollution from extended forest fires in August 2003 was not a part of the emission inventory, we found monthly mean pollution enhancement by a factor of 1.5. On a daily basis, the variation in pollution levels due to meteorological conditions is expected to be even more significant.

[29] Meteorological conditions also substantially influence the formation of secondary aerosol particles. Availability of clouds and liquid water are found to govern sulfate production over northern and central Europe, while temperature and solar radiation to be the main contributors in southern Europe via photo-oxidation processes. The production of secondary organic aerosol in our model is mainly governed by the efficiency of photo-oxidation. To be able to predict pollution levels by modeling the aerosol distribution, accuracy in emission sources, formation processes and simulated meteorological conditions are equally important.

[30] **Acknowledgments.** We thank Benedickt Schell for providing the SORGAM model, Martin Schultz and Ulrike Niemeier for providing the MOZART data, CARBOSOL team and Anne-G. Hjellbrekke for providing observation data, Melissa Pfeffer for reviewing the manuscript internally and Andraś Gelencsér for cooperation and review. This research was financially supported by EU project CARBOSOL.

## References

Andersson-Skøld, Y., and D. Simpson (2001), Secondary organic aerosol formation in northern Europe: A model study, *J. Geophys. Res.*, *106*, 7357–7374.

Bond, T., D. Streets, K. Yarber, S. Nelson, J. Woo, and Z. Klimont (2004), A technology-based global inventory of black and organic carbon emissions from combustion, *J. Geophys. Res.*, *109*, D14203, doi:10.1029/2003JD003697.

Chang, J. S., R. A. Brost, I. S. A. Isaksen, S. Madronich, P. Middleton, W. R. Stockwell, and C. J. Walcek (1987), A three-dimensional Eulerian acid deposition model: Physical concepts and formulation, *J. Geophys. Res.*, *93*, 14,681–14,700.

Claeys, M., B. Graham, and G. Vas (2004), Formation of secondary organic aerosols through photooxidation of isoprene, *Science*, *303*, 1173–1176.

Gelencsér, A., B. May, D. Simpson, A. Sánchez-Ochoa, A. Kasper-Giebl, H. Puxbaum, A. Caseiro, C. Pio, and M. Legrand (2007), Source apportionment of $PM_{2.5}$ organic aerosol over Europe: Primary/secondary, natural/anthropogenic, and fossil/biogenic origin, *J. Geophys. Res.*, *112*, D23S04, doi:10.1029/2006JD008094.

Guenther, A., R. Monson, and R. Fall (1991), Isoprene and monoterpene emission rate variability: Observations with eucalyptus and emission rate algorithm development, *J. Geophys. Res.*, *96*, 10,799–10,808.

Guenther, A., P. Zimmermann, P. Harley, R. Monson, and R. Fall (1993), Isoprene and monoterpene emission rate variability: Model evaluations and sensitivity analyses, *J. Geophys. Res.*, *98*, 12,608–12,617.

Hass, H., A. Ebel, H. Feldmann, H. Jakobs, and M. Memmesheimer (1993), Evaluation studies with a regional chemical transport model (EURAD) using air quality data from the EMEP monitoring network, *Atmos. Environ., Part A*, *27*, 867–887.

Hass, H., H. Jakobs, and M. Memmesheimer (1995), Analysis of a regional model (EURAD) near surface gas concentrations predictions using observations from networks, *Meteorol. Atmos. Phys.*, *57*, 173–200.

Hass, H., M. van Loon, C. Kessler, R. Stern, J. Matthijsen, F. Sauter, Z. Zlatev, J. Langner, V. Foltescu, and M. Schaap (2003), Aerosol modelling: Results and intercomparison from European regional-scale modelling systems. A contribution to the EUROTRAC-2 subproject GLOREAM, technical report, EUROTRAC ISS, Munich, Germany.

Haywood, J., and O. Boucher (2000), Estimates of the direct and indirect radiative forcing due to tropospheric aerosols: A review, *Rev. Geophys.*, *38*, 513–543.

Hesstvedt, E., O. Hov, and I. Isaksen (1978), Quasi steady-state approximations in air pollution modelling: Comparison of two numerical schemes for oxidant prediction, *Int. J. Chem. Kinet.*, *10*, 971–994.

Hitzenberger, R., A. Berner, R. Kromp, A. Kasper-Giebl, A. Limbeck, W. Tscherwenka, and H. Puxbaum (2000), Black carbon and other species at a high-elevation European site (Mount Sonnblick, 3106 m, Austria): Concentrations and scavenging efficiencies, *J. Geophys. Res.*, *105*(D20), 24,637–24,646.

Hjellbrekke, A.-G. (2004), Data report 2002, acidifying and eutrophying compounds, *Tech. Rep. EMEP/CCC Rep. 1/2004*, EMEP, Oslo, Norway.

Hongisto, M., M. Sofiev, and S. Joffre (2003), Hilatar, a limited area simulation model of acid contaminants, part II, *Atmos. Environ.*, *37*, 1535–1547.

Horowitz, L. W., et al. (2003), A global simulation of tropospheric ozone and related tracers: Description and evaluation of MOZART, version 2, *J. Geophys. Res.*, *108*(D24), 4784, doi:10.1029/2002JD002853.

Jacob, D. (2001), A note to the simulation of the annual and inter-annual variability of the water budget over the Baltic sea drainage basin, *Meteorol. Atmos. Phys.*, *77*, 61–73.

Kasper-Giebl, A., A. Koch, R. Hitzenberger, and H. Puxbaum (2000), Scavenging efficiency of "Aerosol Carbon" and sulfate in supercooled clouds at Mt. Sonnblick (3106 m a.s.l.), Austria, *J. Atmos. Chem.*, *35*, 33–46.

Langmann, B. (2000), Numerical modelling of regional scale transport and photochemistry directly together with meteorological processes, *Atmos. Environ.*, *34*, 3585–3598.

Limbeck, A., M. Kulmala, and H. Puxbaum (2003), Secondary organic aerosol formation in the atmosphere via heterogeneous reaction of gaseous isoprene on acidic particles, *Geophys. Res. Lett.*, *30*(19), 1996, doi:10.1029/2003GL017738.

Madronich, S. (1987), Photodissociation in the atmosphere: 1. actinic flux and the effects of ground reflections and clouds, *J. Geophys. Res.*, *92*, 9740–9752.

Mellor, B., and T. Yamada (1974), A hierarchy of turbulence closure models for planetary boundary layers, *J. Atmos. Sci.*, *31*, 1791–1806.

Memmesheimer, M., J. Tippke, A. Ebel, H. Hass, H. Jakobs, and M. Laube (1991), On the use of EMEP emission inventories for European scale air pollution modelling with the EURAD model, paper presented at EMEP Workshop on Photooxidant Modelling for Long-Range Transport in Relation to Abatement Strategies, Berlin, Germany.

Mesinger, F., and A. Arakawa (1976), *Numerical Methods Used in Atmospheric Models*, World Meteorol. Organ., Geneva, Switzerland.

Pio, C., et al. (2007), Climatology of aerosol composition (organic versus inorganic) at nonurban sites on a west-east transect across Europe, *J. Geophys. Res.*, *112*, D23S02, doi:10.1029/2006JD008038.

Putaud, J., et al. (2004), A European aerosol phenomenology—2: Chemical characteristics of particulate matter at kerbsite, urban, rural and background sites in Europe, *Atmos. Environ.*, *38*, 2579–2595.

Roeckner, E. (1996), The atmospheric general circulation model ECHAM4: Model description and simulation of present-day climate, *MPI Rep. 218*, Max-Planck-Inst. für Meteorol., Hamburg, Germany.

Schaap, M., H. A. C. D. Van Der Gon, F. J. Dentener, A. J. H. Visschedijk, M. Van Loon, H. M. ten Brink, J-.P. Putaud, B. Guillaume, C. Liousse, and P. J. H. Builtjes (2004), Anthropogenic black carbon and fine aerosol distribution over Europe, *J. Geophys. Res.*, *109*, D18207, doi:10.1029/2003JD004330.

Schell, B. (2000), Die Behandlung sekundärer organischer Aerosole in einem komplexen Chemie-Transport-Modell, Ph.D. thesis, Univ. of Cologne, Cologne, Germany.

Simpson, D., K. E. Yttri, Z. Klimont, K. Kupiainen, A. Caseiro, A. Gelencsér, C. Pio, H. Puxbaum, and M. Legrand (2007), Modeling carbonaceous

aerosol over Europe: Analysis of the CARBOSOL and EMEP EC/OC campaigns, *J. Geophys. Res.*, *112*, D23S14, doi:10.1029/2006JD008158.
Smolarkiewitz, P. (1983), A simple positive definite advection scheme with small implicit diffusion, *Mon. Weather Rev.*, *111*, 476–479.
Solmon, F., F. Giorgi, and C. Liousse (2006), Aerosol modelling for regional climate studies: Application to anthropogenic particles and evaluation over a European/African domain, *Tellus, Ser. B*, *58B*, 51–72.
Stockwell, W., P. Middleton, J. Chang, and X. Tang (1990), The second generation regional acid deposition model: Chemical mechanism for regional air quality modeling, *J. Geophys. Res.*, *95*, 16,343–16,367.
Stoddard, J., et al. (1999), Regional trends in aquatic recovery from acidification in North America and Europe, *Nature*, *401*, 575–578.
Tiedtke, M. (1989), A comprehensive mass flux scheme for cumulus parameterization in large-scale models, *Mon. Weather Rev.*, *117*, 1778–1800.
van Loon, M., I. Ackermann, M. Schaap, and P. Builtjes (2000), Primary and secondary aerosol simulation using LOTOS, *J. Aerosol Sci.*, *31*, S52–S53.
Vestreng, V. (2003), Review and revision. Emission data reported to CLRTAP, EMEP-MSCW Status Report 2003, *Tech. Rep. Note 1/2003*, Norw. Meteorol. Inst., Oslo, Norway.
Vestreng, V., M. Adams, and J. Goodwin (2004), Inventory review 2004. Emission data reported to CLRTAP and under the NEC directive, EMEP/EEA Joint Review Report, *Tech. Rep. EMEP-MSCW Rep. 1/2004*, Norw. Meteorol. Inst., Oslo, Norway.
Walcek, C. J., R. A. Brost, J. S. Chang, and M. L. Wesely (1986), $SO_2$, sulfate and $HNO_3$ deposition velocities computed using regional landuse and meteorological data, *Atmos. Environ.*, *20*, 949–964.
Wesley, M. (1989), Parameterization of surface resistances to gaseous dry deposition in regional-scale numerical models, *Atmos. Environ.*, *23*, 1293–1304.
World Health Organization (2002), World health report 2002, technical report, Geneva, Switzerland.

B. Langmann, Department of Experimental Physics, National University of Ireland, Galway, Ireland. (baerbel.langmann@zmaw.de)
E. Marmer, Institute for Environment and Sustainability, European Commission–Joint Research Centre, I-21020 Ispra, Italy. (elina.marmer@jrc.it)